Temporal pulse compression by dynamic slow-light tuning in photonic-crystal waveguides

K. Kondo, N. Ishikura, T. Tamura, and T. Baba
Department of Electrical and Computer Engineering, Yokohama National University, 79-5 Tokiwadai, Hodogayaku, Yokohama 240-8501, Japan

(Received 25 November 2014; revised manuscript received 27 January 2015; published 25 February 2015)

We demonstrate on-chip pulse compression based on the dynamic tuning in a copropagating slow-light system. Low-dispersion slow-light control pulse in lattice-shifted photonic-crystal waveguides enhances two-photon absorption. Generating free carriers dynamically through the two-photon absorption so as to sweep a signal slow-light pulse, the spectral broadening occurs with a monotonic chirp. The signal pulse is then compressed through the compensation of the chirp by means of integrated heaters. An input pulse of 13.9 ps length was compressed to 1.4 ps, corresponding to a compression factor of 9.9.

DOI: 10.1103/PhysRevA.91.023831 PACS number(s): 42.70.Qs, 42.25.Bs, 42.79.Nv, 42.82.−m

Lattice-shifted photonic-crystal waveguides (LSPCWs) generate low-dispersion slow-light pulses [1,2] and enhance nonlinear effects [2,3]. Depending on structural parameters, they simultaneously generate slow-light pulses whose group delay and dispersion are tunable [4]. Here, we focus on the copropagating slow-light system, in which the low-dispersion slow light and tunable slow light are used as a control pulse and signal pulse, respectively. Adiabatic wavelength conversion [5–11] and fast delay tuning [12,13] in the signal pulse through the nonlinearity of the control pulse have previously been achieved. In this paper, we demonstrate that pulse compression can also be achieved with spectral broadening by optimizing the two pulses and dispersion of the LSPCW.

Two approaches are well known for optical pulse compression. One is the spectral broadening in optical fibers followed by the dispersion compensation using a pair of gratings [14]. The same approach has also been demonstrated on a chip in Si photonic circuits [15]. The other approach is by generating a soliton pulse [16,17]. Even though they are different in terms of separate or simultaneous spectral broadening and dispersion compensation, both need the spectral broadening with a monotonic chirp [Fig. 1(a)]; in both cases, it is obtained by the optical Kerr effect. In recent years, on-chip pulse compression using a photonic-crystal waveguide (PCW) has been investigated as a result of the advancement of slow light. However, when two-photon absorption (TPA) occurs and free carriers are generated, for example, in Si PCW at telecom wavelengths, carrier plasma dispersion and absorption prevent the formation of the monotonic wavelength chirp and degrade the compression. Soliton compression in a GaInP PCW with a small TPA resulted in a compression factor of 5.2 [18] compared to a factor of only 2.3 in a Si PCW [19]. These small values might also be due to the low flexibility of the process in which the signal pulse tunes itself through the nonlinearity.

In our approach using the copropagating slow-light system in the Si LSPCW, we can improve the flexibility and obtain the spectral broadening with the monotonic chirp by using carrier plasma dispersion instead of the optical Kerr effect. The carrier plasma dispersion is dynamically induced by the TPA of a control pulse; the TPA is enhanced by the spatial compression of the control pulse under the slow-light propagation. The carrier plasma dispersion blueshifts the spectrum of a copropagating signal pulse. Here the control pulse is attenuated by some losses in the propagation. Therefore, when the control pulse slowly overtakes the signal pulse, the amount of the blueshift in the signal pulse is gradually reduced; hence the signal spectrum is broadened from the initial one toward the short-wavelength side resulting in a monotonic chirp [Fig. 1(b)]. Subsequently, the pulse is compressed through the dispersion compensation in the LSPCW whose dispersion is tuned by integrated multiheaters. In this paper, we first show the experimental results and then explain the physical behaviors of the two pulses in detail. We will also discuss the relation between the pulse compression and the other functions of the copropagating slow-light system.

The air-bridge LSPCW with multiheaters is fabricated on the silicon-on-insulator substrate by using a complementary metal-oxide semiconductor (CMOS)–compatible process whose minimum feature size is 180 nm [4], as shown in Fig. 2. The 350-μm-long LSPCW consists of a line defect waveguide in a 210-nm-thick Si photonic-crystal slab with an array of air holes in a triangular lattice (250-nm hole diameter and 450-nm lattice constant). The lattice shift is introduced into third rows of holes on both sides from the line defect to generate the low-dispersion slow light [2,11,13]. Both ends are coupled to external lensed fibers through Si wire waveguides and spot size converters. Seven pairs of TiN heaters are integrated beside the LSPCW and controlled independently by an external controller through Al wires. Figure 3 shows the group delay spectrum of the LSPCW. Without heating (black line), a delay peak appeared at $\lambda \sim 1540$ nm, which corresponds to tunable slow light. The flat spectrum on the long-wavelength side corresponds to low-dispersion slow light. When we applied 125 mW of power to each of the four pairs of heaters on the rear side, the delay peak of the heated area shifted to 1548 nm (red line). The shorter side of the peak was flattened due to the delay peak on the front side averaged by the sloped temperature distribution, while the longer side corresponds to the low-dispersion slow-light band that has been redshifted by the heating. At these heating conditions, we launched the signal and control pulses on the LSPCW at peak wavelengths of λ_s and λ_c, respectively. At this λ_s, the passive loss in the LSPCW in the absence of the control pulse was estimated to be 7 dB. Synchronized signal and control pulses with wanted pulse lengths and peak wavelengths were produced using a mode-locked fiber laser, two band-pass filters, an optical attenuator, and a mechanically tunable delay line. The wave form and spectrum of input and output pulses were measured

 ©2015 American Physical Society

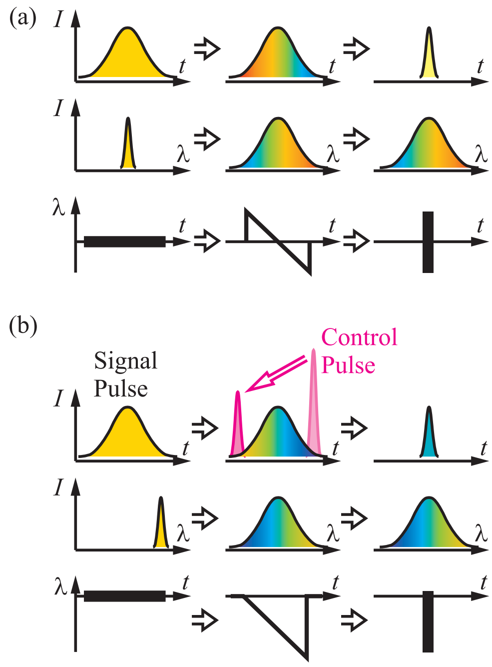

FIG. 1. (Color online) Pulse compression processes. (a) Conventional approach using the optical Kerr effect of the signal pulse itself. I is the intensity, λ is the wavelength, and t is the time. (b) Our approach based on a copropagating slow-light system.

by cross-correlator and optical spectrum analyzer, respectively. The pulse length was evaluated as the full width at half maximum (FWHM) of the wave form after deconvoluting from a reference pulse, assuming either Gaussian or sech^2 profile, which gives a better fit. The detail of the optical setup was the same as those for the adiabatic wavelength conversion [11] and the fast delay tuning [13]. However, as discussed below, we set the signal pulse length to be longer and control pulse length to be shorter than those in Ref. [11]; i.e., the length and the peak power of the signal pulse are 13.9 ps and 0.3 W, respectively, compared to 5.7 ps and 13 W for the control pulse.

Experimental results are summarized in Fig. 4. Figure 4(a) shows the cross-correlation wave form of the output signal pulse for a reference pulse, color map, and pulse length $\Delta\tau_s$ as a function of the relative input timing of the control pulse Δt_0. The white solid line on this color map indicates the output timing of the control pulse. The signal pulse is sharpened along with this line. $\Delta\tau_s$ takes its minimum value of 1.9 ps for $\Delta t_0 =$ 0.5–2.5 ps, corresponding to a compression factor of 7.0.

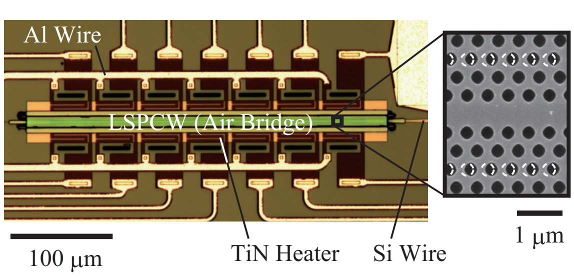

FIG. 2. (Color online) Top view of LSPCW with multiheaters used in our experiment.

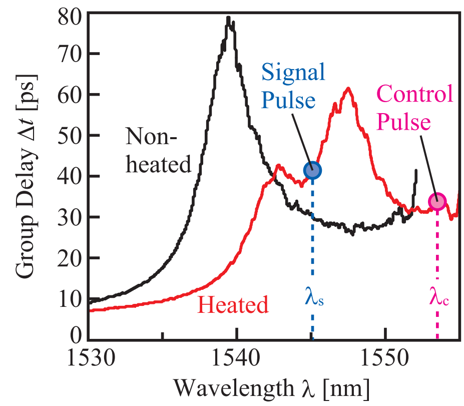

FIG. 3. (Color online) Group delay spectrum of the LSPCW measured by the modulation phase-shift method.

Figure 4(b) shows the spectral profile, color map, and width $\Delta\lambda$. Here, the full widths at -3 and -10 dB of the spectral peak are employed as $\Delta\lambda$. The $\Delta\lambda_{-3\text{dB}}$ does not increase so much although the temporal pulse length is compressed at $\Delta t_0 > 0.5$ ps. Here, $\Delta\lambda_{-3\text{dB}}$ is dominated by the residual unchanged spectral components having a narrower width and higher peak, which is not the spectral behavior of interest. At $\Delta t_0 < 0.5$ ps, the spectral broadening in $\Delta\lambda_{-3\text{dB}}$ becomes clear due to the absorption of the unchanged components by free carriers, but still the unchanged components have an influence. Therefore, $\Delta\lambda_{-10\text{dB}}$, which can eliminate the influence, exhibits the spectral broadening more reasonably. The spectral oscillation that might be caused by the passive transmission spectrum of the LSPCW is observed in the profile and color map. Neglecting the oscillation, $\Delta\lambda_{-10\text{dB}}$ evaluated from the envelope increases from 0.53 nm at the input end to 4.67 nm at the output end. The broadening mainly occurred toward the short-wavelength side because of the dynamic tuning due to the TPA-induced free carriers; however, a slight broadening is also seen toward the long-wavelength side. The redshifted components at Δt_0 from -2 to 8 ps might be due to the optical Kerr effect, which is known to occur at the leading edge of the control pulse. On the other hand, that at $\Delta t_0 < -2$ ps might be due to the depletion (diffusion) of carriers, which is the reverse process of the blueshift due to the generation of carriers. Figure 4(c) shows the peak power and integrated power of the signal pulse normalized by their values without the control pulse. The reduction of the integrated power at small Δt_0 is mainly caused by the free-carrier absorption. At $\Delta t_0 = 2.5$ ps, the integrated power is reduced to 0.45 times, which adds 3.5 dB loss to the above-mentioned 7 dB passive loss. However, the peak power is enhanced up to 2.6 times with the pulse compression. A similar compression is observed at Δt_0 from -2 to 7 ps, whereas a smaller loss is observed at larger Δt_0. We estimated the TPA-induced free-carrier density from the equations derived in [3,20] to be of 2×10^{18} cm^{-3} order ($\Delta n \sim -0.006$) at the input end where the control pulse has the highest intensity, while of 10^{16} cm^{-3} order ($\Delta n \sim -0.0001$) order at the output end, due to the attenuation of the intensity.

We repeated the same measurement for many device samples and observed the similar behaviors of the pulse wave

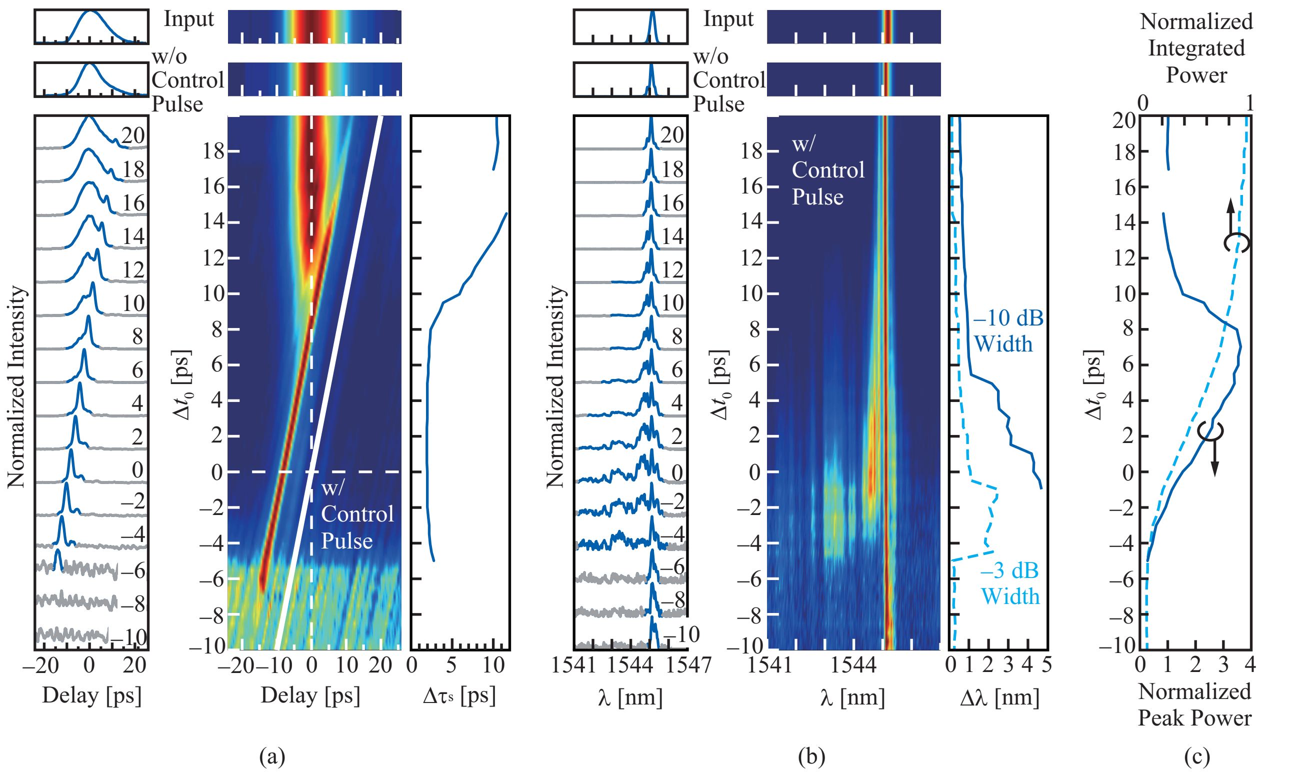

FIG. 4. (Color online) Experimental results. (a) Cross-correlation wave form (FWHM of the reference pulse is 0.5 ps), color map, and $\Delta\tau_s$ (FWHM after deconvolution) of output signal pulse. (b) Spectral profile, color map, and $\Delta\lambda$ corresponding to (a). (c) Peak power and integrated power corresponding to (a). Intensities in (a) and (b) are normalized by their maxima. Integrated and peak powers in (c) are normalized by their values observed without control pulse. Input timing of the control pulse Δt_0 is defined as the delay of the control pulse peak against the signal pulse peak at the input end. The white solid line in (a) shows the timing of the control pulse peak at the input end.

form and spectrum. Figure 5 shows the pulse wave forms showing the highest compression factor of 9.9; a 13.9-ps pulse was compressed to 1.4 ps. This compression factor is higher than those reported previously for any on-chip pulse compression.

We analyze the behaviors of the pulses in the LSPCW and consider the observed pulse compression. The time-space relation between the two pulses depends on the input wavelengths in the group delay spectrum of the LSPCW, the heating power, and the temperature distribution. The group

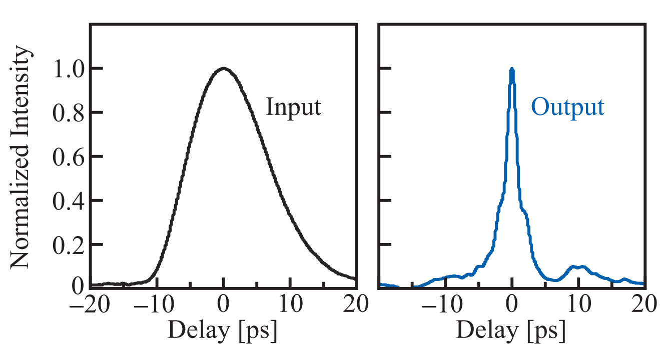

FIG. 5. (Color online) Cross-correlation wave forms of input and output signal pulse showing the highest pulse compression factor. Their lengths $\Delta\tau_s$ after deconvoluting from 1.2-ps reference pulse are 13.9 and 1.4 ps, respectively.

delay spectrum of LSPCWs, $\Delta t(\lambda)$, is expressed as

$$\Delta t(\lambda) = \int_0^L \frac{\partial t\,[\lambda(z) - a\Delta T(z)]}{\partial z} dz, \quad (1)$$

where L is the LSPCW length, $\partial t/\partial z$ is the local delay given by the group delay of the nonheated condition, $\lambda(z)$ is the local wavelength considering the dynamic tuning, $\Delta T(z)$ is the local temperature shift due to the heaters, and a is a spectrum-temperature coefficient. The timing difference of the two pulses, $\Delta t_{\mathrm{s-c}}$, at z is given by

$$\Delta t_{\mathrm{s-c}}(z) = \int_0^z \left\{ \frac{\partial t\,[\lambda_{\mathrm{s}}(z) - a\Delta T(z)]}{\partial z} - \frac{\partial t\,[\lambda_{\mathrm{c}} - a\Delta T(z)]}{\partial z} \right\} \times dz - \Delta t_0. \quad (2)$$

For these formulas, we first determine $\Delta T(z)$ by fitting the calculated $\Delta t(\lambda)$ with the experimental one, considering $a = 0.082$ nm/K, as reported for the Si LSPCW [7]. When we assume $\Delta T(z)$ under the heating condition as that shown in Fig. 6(a), $\Delta t(\lambda)$ calculated from Eq. (1) becomes that depicted by the gray line in Fig. 6(b); this also agrees well with the experimentally measured $\Delta t(\lambda)$ (red line). Here, ΔT at the nonheated region ($z < 125\ \mu$m) becomes ~40 K due to thermal diffusion. The local group delay spectra are arranged along z based on the $\Delta T(z)$ in Fig. 6(c), where the evolution of the pulses' spectra are overlaid. While the control pulse continues to propagate in the low-dispersion band, the signal pulse is influenced by the dynamic tuning during the

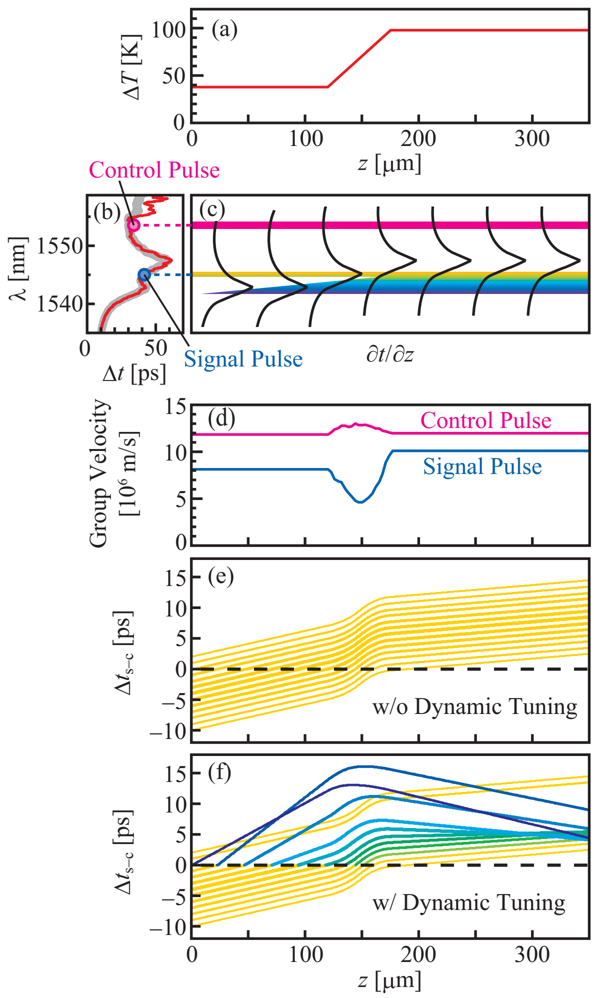

FIG. 6. (Color online) Analysis of the pulse compression. (a) Assumed temperature distribution. (b) Calculated group delay spectrum (pale tone line) and measured spectrum (deep tone line). (c) Local group delay spectrum and spectra of two pulses. (d) Variation in group velocities of two pulses in LSPCW. (e), (f) Relative delay, Δt_{s-c}, of signal pulse components with 1-ps interval. $\Delta t_0 = -4$ ps and $\Delta\tau_s = 12$ ps are assumed. The positive value of Δt_{s-c} shows that the signal pulse is delayed from the control pulse. The change of line color beyond $\Delta t_{s-c} = 0$ schematically expresses the blueshift due to the dynamic tuning.

propagation in the positive-dispersion region and then begins to propagate in the negative-dispersion region with a temporary high group velocity and small local delay. The corresponding variations in group velocities of the signal and control pulses at the their input wavelengths are estimated, as shown in Fig. 6(d). Note that it does not take account of the signal's spectral shift due to the dynamic tuning. Furthermore, Fig. 6(e) shows Δt_{s-c}, given by Eq. (2), if there were no dynamic tuning and dispersion. In this case, we set $\Delta t_0 = 4$ ps, as an example, and express the signal pulse length of ± 6 ps from the peak by multiple lines whose thickness is schematically weighted by the temporal intensity. The change in Δt_{s-c} from negative values to 0 indicates that the signal pulse is caught up by the control pulse. The steplike behavior near the midpoint arises from the signal spectrum sliding over the delay peak due to the temperature slope. With no dynamic tuning and dispersion, the length of the signal pulse does not change between the input and output. On the other hand, when the signal pulse is blueshifted by the dynamic tuning, the behavior changes, as shown in Fig. 6(f). Here, we simplified the situation such that each temporal component of the signal pulse is blueshifted when it overlaps with the control pulse peak ($\Delta t_{s-c} = 0$). Since the control pulse is attenuated mainly due to the TPA and the free-carrier absorption, we consider that the amount of the blueshift $\Delta\lambda_s = \Delta\lambda_{s0}$ at the input end decreases in inverse proportion to z^2 and vanishes at $z > z_0$; i.e.,

$$\Delta\lambda_s(z) = \Delta\lambda_{s0}(1 - z/z_0)^2. \quad (3)$$

We experimentally estimated the values of $\Delta\lambda_{s0}$ and z_0 to be -3.5 nm and 160 μm, respectively. The signal pulse components overlap at $\Delta t_{s-c} = 0$ from the back end in sequence; thus, the blueshift is gradually reduced from the back end to the front end, forming a monotonic wavelength chirp, as depicted in Fig. 1(b). The chirped pulse is broadened in the positive-dispersion region. It is then focused in the negative-dispersion region at $z > 175\,\mu$m and compressed around the point where $\Delta t_{s-c} = 5$ ps at the output end. According to Fig. 6(f), the pulse duration within ± 4 ps contributes to the compression, whereas the outer components do not. However, some outer components do contribute to the compression because the control pulse has a finite length. The experimental results are well explained by Fig. 6(f).

As the signal pulse is as long as 13.9 ps at the input end, similar pulse compression occurs in the range of approximately $-5 < \Delta t_0 < 5$ ps. However, the front end and back end of the signal pulse are not involved in the compression for other Δt_0. Note that the integrated pulse intensity is greatly reduced at $-5 < \Delta t_0 < 0$ ps [Fig. 4(c)]. In this situation, signal components launched later than the control pulse are attenuated by the free-carrier absorption, which might look like a more compressed pulse.

Finally, let us summarize the functions achieved by means of the dynamic tuning in the copropagating slow-light system. Previously, we have reported large adiabatic wavelength shift [11] and fast delay tuning [13] using this system. The pulse compression fundamentally utilizes the same system, but

TABLE I. (Color online) Three functions produced by dynamic tuning in copropagating slow-light system.

Function	Signal spectrum	Pulse length relation	Signal dispersion
Wavelength conversion [11]	Simply shifted	Signal, Control	Unnecessary
Fast delay tuning [13]	Simply shifted	Signal, Control	Necessary
Pulse compression	Expanded	Signal, Control	Necessary

the main differences are in the setting of pulse length and wavelength, as summarized in Table I. As pure spectral shift without broadening is desired in the adiabatic wavelength shift, the dynamic index change should be applied uniformly to all the signal components. For this purpose, a low-dispersion signal pulse and a long control pulse are effective. The fast delay tuning also uses similar wavelength shifts but needs the dispersion in the signal pulse for changing the output timing. Moreover, the control pulse used as a timing clock needs to be short enough for the fast response. Therefore, the optimum length of the control pulse is the same as that of the signal pulse. In contrast, the pulse compression is obtained in the spectral broadening process, whereby the short control pulse sweeps the signal pulse, and the dispersion compensation. Such a variety in pulse length, group velocity and dispersion, as well as the enhanced nonlinearities, are achieved by the LSPCW and the large flexibility of slow light. The dynamic tuning in the copropagating slow-light system of the LSPCW is expected to additionally produce other functions.

This study was partly supported by the New Energy and Industrial Technology Development Organization.

[1] J. Li, T. P. White, L. O'Faolain, A. Gomez-Iglesias, and F. Krauss, Opt. Express **16**, 6227 (2008).
[2] Y. Hamachi, S. Kubo, and T. Baba, Opt. Lett. **34**, 1072 (2009).
[3] C. Monat, B. Corcoran, M. Ebnali-Heidari, C. Grillet, B. J. Eggleton, T. P. White, L. O'Faolain, and T. F. Krauss, Opt. Express **17**, 2944 (2009).
[4] N. Ishikura, R. Hayakawa, R. Hosoi, T. Tamanuki, M. Shinkawa, and T. Baba, Appl. Phys. Lett. **100**, 221110 (2012).
[5] M. F. Yanik and S. Fan, Phys. Rev. Lett. **92**, 083901 (2004).
[6] M. Notomi and S. Mitsugi, Phys. Rev. A **73**, 051803 (2006).
[7] S. F. Preble, Q. Xu, and M. Lipson, Nat. Photonics **1**, 293 (2007).
[8] T. Kampfrath, D. M. Beggs, T. P. White, A. Melloni, T. F. Krauss, and L. Kuipers, Phys. Rev. A **81**, 043837 (2010).
[9] D. M. Beggs, T. F. Krauss, L. Kuipers, and T. Kampfrath, Phys. Rev. Lett. **108**, 033902 (2012).
[10] M. C. Muñoz, A. Y. Petrov, and M. Eich, Appl. Phys. Lett. **101**, 141119 (2012).
[11] K. Kondo and T. Baba, Phys. Rev. Lett. **112**, 223904 (2014).
[12] D. M. Beggs, I. H. Rey, T. Kampfrath, N. Rotenberg, L. Kuipers, and T. F. Krauss, Phys. Rev. Lett. **108**, 213901 (2012).
[13] K. Kondo, M. Shinkawa, Y. Hamachi, Y. Saito, Y. Arita, and T. Baba, Phys. Rev. Lett. **110**, 053902 (2013).
[14] H. Nakatsuka, D. Grischkowsky, and A. C. Balant, Phys. Rev. Lett. **47**, 910 (1981).
[15] D. T. H. Tan, P. C. Sun, and Y. Fainman, Nat. Commun. **1**, 116 (2010).
[16] G. P. Agrawal, *Nonlinear Fiber Optics*, 4th ed. (Academic, Boston, 2007).
[17] J. C. Travers, J. M. Stone, A. B. Rulkov, B. A. Cumberland, A. K. George, S. V. Popov, J. C. Knight, and J. R. Taylor, Opt. Express **15**, 13203 (2007).
[18] P. Colman, C. Husko, S. Combrié, I. Sagnes, C. W. Wong, and A. D. Rossi, Nat. Photonics **4**, 862 (2010).
[19] A. Blanco-Redondo, C. Husko, D. Eades, Y. Zhang, J. Li, T. F. Krauss, and B. J. Eggleton, Nat. Commun. **5**, 3160 (2014).
[20] R. A. Soref and B. R. Bennett, IEEE J. Quantum Electron. **23**, 123 (1987).